



Cite this: *Phys. Chem. Chem. Phys.*,  
2015, 17, 22659

# Multifunctional MWCNTs–NaGdF<sub>4</sub>:Yb<sup>3+</sup>,Er<sup>3+</sup>,Eu<sup>3+</sup> hybrid nanocomposites with potential dual-mode luminescence, magnetism and photothermal properties

Wenjia Liu, Guixia Liu,\* Xiangting Dong, Jinxian Wang and Wensheng Yu

A novel dual-mode luminescence multifunctional hybrid nanomaterial has been successfully prepared by coating the NaGdF<sub>4</sub>:Yb<sup>3+</sup>,Er<sup>3+</sup>,Eu<sup>3+</sup> nanoparticles (NPs) on the surface of MWCNTs. The as-synthesized MWCNTs–NaGdF<sub>4</sub>:Yb<sup>3+</sup>,Er<sup>3+</sup>,Eu<sup>3+</sup> nanocomposites (NCs) can simultaneously take advantage of both magnetic and optical properties of NaGdF<sub>4</sub>:Yb<sup>3+</sup>,Er<sup>3+</sup>,Eu<sup>3+</sup> NPs and the photothermal conversion property of MWCNTs. The samples were characterized by X-ray diffraction (XRD), scanning electron microscopy (SEM), energy-dispersive X-ray spectrometry (EDS), vibrating sample magnetometry (VSM), UV-Vis absorption, luminescence spectroscopy and fluorescence lifetime measurements. Meanwhile, the photothermal conversion was examined under irradiation with a 980 nm laser. The results show that the MWCNTs–NaGdF<sub>4</sub>:Yb<sup>3+</sup>,Er<sup>3+</sup>,Eu<sup>3+</sup> NCs have preferably magnetic, dual-mode (up- and down-conversion) luminescence and photothermal properties. And the NCs have good biocompatibility, low toxicity and up-conversion luminescence for cell imaging. As a consequence, the dual-mode luminescence multifunctional nanomaterials have potential applications in environmental science fields and clinical fields for magnetic resonance imaging, fluorescence imaging, photothermal therapy, bioseparation and targeted drug delivery.

Received 28th June 2015,  
Accepted 28th July 2015

DOI: 10.1039/c5cp03725e

[www.rsc.org/pccp](http://www.rsc.org/pccp)

## 1 Introduction

Carbon nanotubes (CNTs), first discovered in 1991,<sup>1</sup> have been considered as attractive carbon nanomaterials due to their high surface area and chemical, optical, mechanical, electronic and photothermal conversion properties.<sup>2–6</sup> In recent years, a number of studies in the field of nanomedicine and nanotechnology have proved that CNTs play a key role in a variety of areas, such as drug and gene delivery, sensor devices, sewage treatment, separation processes and environmental governance.<sup>7–13</sup> In particular, the photothermal conversion property of CNTs allows their use for potential biological application in thermotherapy to cancer cells. Meanwhile, the near-infrared (NIR) light has deeper tissue penetration and fascinating heating effect, which are widely used for photothermal therapy (PTT) in biomedical fields. The programmer localizes the optical absorption agents at the cancer site and irradiates the site with the NIR light to “bake” the cancer cells, because blood and tissues in the NIR light region have the lowest absorption, and the implementation is noninvasive and relatively simple.<sup>14–16</sup> As we all have known that noble metal nanoparticles

and CNTs have always acted as absorption agents to improve the photothermal effect in the NIR light region,<sup>17,18</sup> they can convert the NIR light to heat through the photothermal conversion effect.<sup>19</sup> However, the surface of noble metal nanoparticles is difficult to be modified and they are toxic to human bodies, while the CNTs have low price, high surface area and one-dimensional hollow structure, which can provide an ideal platform for bonding various chemical groups and medicines on the external surface or inside, and some in-depth research is still ongoing. CNTs include single-walled carbon nanotubes (SWCNTs) and multi-walled carbon nanotubes (MWCNTs).<sup>20–22</sup> In contrast to SWCNTs, MWCNTs can remarkably absorb more NIR light, because of the fact that the MWCNTs contain more metallic tubes and have more electrons available for absorbing per particle compared to SWCNTs per weight.<sup>23</sup> Therefore, MWCNTs are frequently used as outstanding candidates for photothermal therapy in clinical applications.<sup>24,25</sup>

CNTs-based multifunctional nanomaterials, emerging as a new generation of engineered nanomaterials, have attracted considerable interest over the years. One example of this is to endow them with optical properties, which has been effected through the combination of conventional luminescent materials with CNTs such as semiconductor quantum dots, organic dyes, inorganic and fluoride nanocrystals. Moreover, the rapid photo-bleaching of organic dyes, the intermittent fluorescence and the

Key Laboratory of Applied Chemistry and Nanotechnology at Universities of Jilin Province, Changchun University of Science and Technology, Changchun 130022, P. R. China. E-mail: liuguixia22@163.com; Fax: +86-431-85383815; Tel: +86-431-85582574

potential toxicity of semiconductor quantum dots further limit their practical applications. Compared to semiconductor quantum dots and organic dyes,  $\text{AREF}_4$  ( $\text{A}$  = alkali metal,  $\text{RE}$  = rare earth,  $\text{F}$  = fluoride) have been looked upon as excellent up- and down-conversion luminescent host materials, including  $\text{NaYF}_4$ ,  $\text{NaGdF}_4$ ,  $\text{KGdF}_4$ ,  $\text{LiGdF}_4$  and so on, which show intrinsic advantages such as low toxicity, low photobleaching, low phonon energies, high quantum yields, high chemical stabilities, high refractive index and a large Stokes shift.<sup>26,27</sup> Another example of this is to endow them with magnetic properties, which has been realized through the combination of supraparamagnetic iron oxide nanoparticles with CNTs that can provide a high spatial resolution of magnetic resonance imaging (MRI). Recently, the  $\text{Gd}^{3+}$  ions have always been used as ideal paramagnetic relaxation agents due to their large magnetic moment and nanosecond time scale electronic relaxation time,<sup>28</sup> which may bring about the longitudinal relaxation ( $r_1$ ) of a water proton, and therefore they have been known as one of the most outstanding  $T_1$ -MRI contrast agents.<sup>29–31</sup> The optical/magnetic multifunctional materials have been prepared, such as  $\text{NaLuF}_4:\text{Gd}^{3+},\text{Yb}^{3+},\text{Er}^{3+}$  nanorods,<sup>32</sup> lanthanide-doped  $\text{KGdF}_4$  nanoparticles,<sup>29</sup> and  $\text{NaGdF}_4:\text{Tb}^{3+},\text{Sm}^{3+}$  nanoparticles.<sup>33</sup> Among the lanthanide doped fluoride materials, luminescent lanthanide ion-doped  $\text{Gd}^{3+}$ -containing NPs have been widely established as a promising new class of multifunctional materials, owing to their excellent magnetic and optical properties. Accordingly,  $\text{NaGdF}_4$  NPs are selected as host nanomaterials, because of their optical and magnetic properties, as well as biocompatibilities, which make them suitable for bioimaging, fluorescence labeling, and bioseparation in environmental science fields and other relevant fields.

In addition to the above mentioned materials, some research groups have devoted themselves to the development of novel dual-mode (up- and down-conversion) luminescence of nanomaterials; in this way, they can expand the scope of application of the materials. For example, the dual-mode luminescence of co-doped  $\text{Yb}^{3+}$  and  $\text{Tb}^{3+}$  ions has been investigated in some inorganic hosts, such as  $\text{GdPO}_4$ ,<sup>34</sup>  $\text{YPO}_4$ ,<sup>35</sup> and  $\text{NaCeF}_4$ ,<sup>36</sup> but the up-conversion emission is too weak to use in practice. In the  $\text{Yb}^{3+},\text{Er}^{3+},\text{Eu}^{3+}$  tri-doped nanocrystal system, the lanthanide dopant  $\text{Eu}^{3+}$  ions reveal merits for use as emitters due to their high quantum efficiency of emission related to the large energy gap between the emitting state and the low lying  $^7\text{F}_J$  ( $J = 0, 1, \dots, 7$ ) excited states and narrow emission lines,<sup>37–39</sup> and the  $\text{Yb}^{3+},\text{Er}^{3+}$  co-doped nanocrystals have been generally investigated as up-conversion emission materials because they can convert the NIR light to green and red emission *via* a dual- or multi-photo mechanism.<sup>40–42</sup> In this case, some researchers have paid attention to the up-conversion luminescence and the energy transfer process of samples, but ignored the down-conversion luminescence. For example, Rai *et al.* studied the up-conversion luminescence of  $\text{Y}_2\text{O}_3:\text{Er}^{3+},\text{Eu}^{3+},\text{Yb}^{3+}$  phosphor and investigated the co-doping influence of  $\text{Yb}^{3+}$  ions.<sup>43</sup> Wang *et al.* successfully synthesized the  $\text{NaYF}_4:\text{Yb}^{3+},\text{Er}^{3+},\text{Eu}^{3+}$  nanocrystals and researched the energy transfer process of the up-conversion.<sup>44</sup> Herein, we focus on the dual-mode luminescence in the  $\text{Yb}^{3+},\text{Er}^{3+},\text{Eu}^{3+}$  tri-doped  $\text{NaGdF}_4$  NP system. Upon excitation

with UV or NIR light, we can acquire down- or up-conversion luminescence, respectively, thus the multifunctional nanomaterials would have potential applications in optical fields. From above all, we choose  $\text{NaGdF}_4:\text{Yb}^{3+},\text{Er}^{3+},\text{Eu}^{3+}$  nanoparticles with magnetic, up- and down-conversion luminescence properties, and MWCNTs with photothermal property to form a multifunctional hybrid nanomaterial.

In the present work, we report a facile and novel route to synthesize a new kind of multifunctional nanomaterial MWCNTs- $\text{NaGdF}_4:\text{Yb}^{3+},\text{Er}^{3+},\text{Eu}^{3+}$  nanocomposites (NCs) with magnetic, photothermal and dual-mode optical properties. At the same time,  $\text{Yb}^{3+},\text{Er}^{3+}$ , and  $\text{Eu}^{3+}$  ions tri-doped  $\text{NaGdF}_4$  NPs can realize up- and down-conversion luminescence under different excitation wavelengths, as well as magnetic properties. To examine the photothermal conversion properties of MWCNTs- $\text{NaGdF}_4:\text{Yb}^{3+},\text{Er}^{3+},\text{Eu}^{3+}$  NCs, they were illuminated under excitation with a 980 nm laser for 10 min. The multifunctional MWCNTs- $\text{NaGdF}_4:\text{Yb}^{3+},\text{Er}^{3+},\text{Eu}^{3+}$  NCs with magnetic, thermal and optical properties may be used for MRI, photothermal therapy and dual-mode luminescence in the biomedical and environmental science fields.

## 2 Experimental section

### 2.1 Chemicals

Gadolinium oxide ( $\text{Gd}_2\text{O}_3$ ), ytterbium oxide ( $\text{Yb}_2\text{O}_3$ ), europium oxide ( $\text{Eu}_2\text{O}_3$ ), erbium oxide ( $\text{Er}_2\text{O}_3$ ), sodium fluoride (NaF), polyvinylpyrrolidone (PVP,  $K = 30$ ), nitric acid ( $\text{HNO}_3$ ), ethylene glycol (EG) and ethanol were purchased from Sinopharm Chemical Reagent Co., Ltd and MWCNTs (purity > 95%) were purchased from Shenzhen Nanotech Port Co., Ltd. Ethylene glycol (EG) and deionized water (DI water) were used as the common solvent in this experiment. All the chemical reagents were of analytical grade and used as received without further purification. Aqueous solution of  $\text{RE}(\text{NO}_3)_3$  ( $\text{RE} = \text{Gd, Yb, Er, Eu}$ ) was obtained by dissolving the rare earth oxides  $\text{RE}_2\text{O}_3$  in dilute  $\text{HNO}_3$  solution (15 mol L<sup>-1</sup>) under heating with agitation in an ambient atmosphere by evaporating the water and adding a certain amount of ethylene glycol (EG).

### 2.2 Synthesis of MWCNTs- $\text{NaGdF}_4:\text{Yb}^{3+},\text{Er}^{3+},\text{Eu}^{3+}$ nanocomposites (NCs)

In a facile method, 7 mg of MWCNTs were added to DI water by sonication to form a homogeneous solution. And 2.0 mmol of  $\text{RE}(\text{NO}_3)_3$  which included  $\text{Gd}(\text{NO}_3)_3$  (1.48 mmol),  $\text{Yb}(\text{NO}_3)_3$  (0.4 mmol),  $\text{Er}(\text{NO}_3)_3$  (0.04 mmol) and  $\text{Eu}(\text{NO}_3)_3$  (0.08 mmol) were added into a 250 mL three-necked flask. After vigorous stirring for 30 min, 2 g of PVP ( $K = 30$ ) and 30 mL of EG were added into the above solution. With additional agitation for 30 min, 10 mL of 2.4 mmol mL<sup>-1</sup> NaF was added dropwise into the above solution. Thereafter, the solution was vigorously stirred until it forms a homogeneous solution under Ar gas flow. Then, the reaction temperature was increased to 180 °C, and the solution was refluxed for 3.5 h before cooling down to room temperature under Ar gas flow. The NCs were separated

by centrifugation at 8000 rpm for 10 min. The products were washed with DI water and ethanol in sequence three times each, and dried in air at 60 °C for 24 h.

### 2.3 Cytotoxicity assay

The cytotoxicity was evaluated by the colorimetric assay by using 3-(4,5-dimethylthiazol-2-yl)-2,5-diphenyltetrazolium bromide (MTT) assay on Hep-2 cells. Hep-2 cells were plated at a density of  $5 \times 10^4$  cells per well in 96-well plates under a humidified 5% CO<sub>2</sub> atmosphere at 37 °C for 24 h, followed by the addition of MWCNTs-NaGdF<sub>4</sub>:Yb<sup>3+</sup>,Er<sup>3+</sup>,Eu<sup>3+</sup> NCs with different concentrations to the medium and incubated for another 24 h. The cells were cultured without materials which were chosen as controls, and each concentration was examined in 3 wells. After that, the cells were washed several times with phosphate buffered saline (PBS) and treated with MTT solution at 37 °C for 4 h in an incubator with 5% CO<sub>2</sub>. MTT was removed and 150 μL of dimethyl sulphoxide (DMSO) was added to each well. Finally, the optical density was measured at 490 nm using an absorbance microplate reader. The cell viability was calculated using the following equation: cell viability (%) = (absorbance of treated wells – absorbance of medium control wells)/(absorbance of untreated wells – absorbance of medium control wells) × 100%.

### 2.4 Characterization

The crystallization and the phase structure of the as-synthesized products were examined by X-ray powder diffraction (XRD) using a Bruker D8 FOCUS with Cu K $\alpha$  radiation ( $\lambda = 1.54056 \text{ \AA}$ ). The morphology and the composition of the products were examined using a field emission scanning electron microscope (FESEM) equipped with an energy-dispersive X-ray spectrometer (EDS). The UV-Vis absorption spectra were obtained on a Shimadzu UV-2450 spectrophotometer. The measurements of photoluminescence and luminescence decay curves were examined on a HITACHI F-7000 at room temperature using a 150 W Xe-lamp as the excitation source. The up-conversion emission spectra were acquired on a HITACHI F-7000 fluorescence spectrophotometer coupled with a 980 nm laser source. Magnetization as a function of the applied magnetic field ranging from -20 to 20 kOe was examined using a vibrating sample magnetometer (VSM) at room temperature. And the temperature of the solution was acquired using a HTC3500C sensitive thermometer. And the solution of products was placed in quartz cuvettes and irradiated with a 980 nm near-infrared (NIR) laser ( $1.2 \text{ W cm}^{-2}$ ) for 10 min. The up-conversion luminescence microscopy (UCLM) instrument was rebuilt on an inverted fluorescence microscope (Nikon Ti-S), and an external CW 980 nm laser diode was used to illuminate the products.

## 3 Results and discussion

### 3.1 Structure and morphology

In order to investigate the composition and the structure of the nanocomposites, the XRD patterns of NaGdF<sub>4</sub>:Yb<sup>3+</sup>,Er<sup>3+</sup>,Eu<sup>3+</sup> NPs (a), MWCNTs (b) and MWCNTs-NaGdF<sub>4</sub>:Yb<sup>3+</sup>,Er<sup>3+</sup>,Eu<sup>3+</sup>

NCs (c) have been recorded from 10° to 60° range as shown in Fig. 1. Fig. 1a displays the peaks at 17.0°, 29.6°, 30.0°, 34.4°, 38.8°, 42.7°, 46.0°, 52.8° and 53.4° corresponding to the (100), (110), (101), (200), (111), (201), (210), (211) and (102) lattice planes of NaGdF<sub>4</sub>, which can be matched with the standard hexagonal phase of NaGdF<sub>4</sub> (JCPDS card 27-0699) and no other diffraction peaks are detected, indicating that the tri-doped Yb<sup>3+</sup>,Er<sup>3+</sup>, and Eu<sup>3+</sup> ions have no impact on the crystal phase structure of the host. However, compared with the standard data, the examined XRD peaks have a slight shift to larger angles, owing to the doped ions occupying sites in the host depending on the effective radii of Yb<sup>3+</sup> (1.182 Å for CN = 9), Er<sup>3+</sup> (1.202 Å for CN = 9) and Eu<sup>3+</sup> (1.260 Å for CN = 9) ions are smaller than those of the Gd<sup>3+</sup> (1.247 Å for CN = 9) ions. From Fig. 1b, it can be seen that the strong peak of MWCNTs corresponds well with the literature value of carbon (PDF card No. 75-0444), which is indexed to the (111) plane. As shown in Fig. 1c, the green circles denote the peaks of the NaGdF<sub>4</sub>:Yb<sup>3+</sup>,Er<sup>3+</sup>,Eu<sup>3+</sup> NPs, and the red asterisk denotes the peak of the MWCNTs. The result indicates that the MWCNTs and NaGdF<sub>4</sub>:Yb<sup>3+</sup>,Er<sup>3+</sup>,Eu<sup>3+</sup> NPs coexist in the nanocomposites.

The morphology and the size of the NaGdF<sub>4</sub>:Yb<sup>3+</sup>,Er<sup>3+</sup>,Eu<sup>3+</sup> NPs, MWCNTs and MWCNTs-NaGdF<sub>4</sub>:Yb<sup>3+</sup>,Er<sup>3+</sup>,Eu<sup>3+</sup> NCs were identified by SEM images. From Fig. 2a, we observed that the NPs are nearly spherical in shape and the sizes are relatively uniform with a mean diameter of 25 nm (Fig. 2b). And the PVP is helpful to disperse the NaGdF<sub>4</sub>:Yb<sup>3+</sup>,Er<sup>3+</sup>,Eu<sup>3+</sup> NPs. The SEM image of MWCNTs is shown in Fig. 2c, the MWCNTs with an average diameter of about 40–60 nm and the length about 2 μm could be observed. Meanwhile, they are well graphitized walls without any other noteworthy coverage materials. From Fig. 2d and e, we can see that the NPs are successfully coated on the surface of MWCNTs. The NCs have a relatively rough surface, which can be easy to modify and improve the photothermal

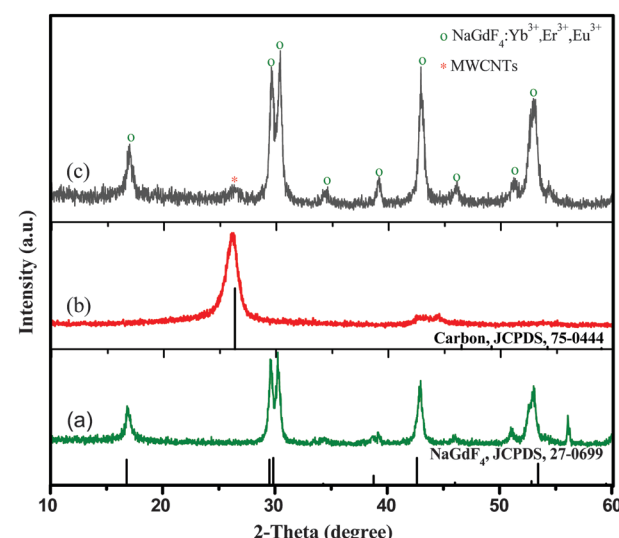
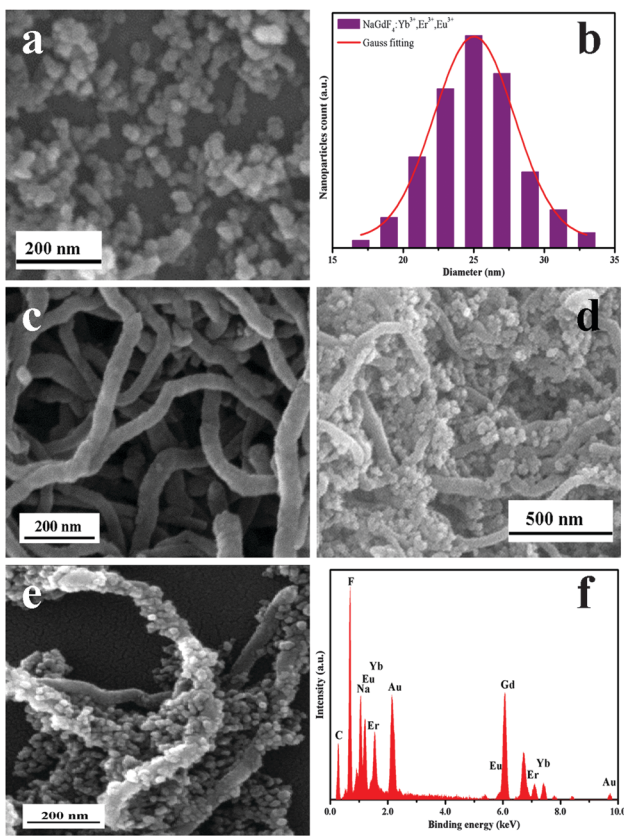


Fig. 1 XRD patterns of NaGdF<sub>4</sub>:Yb<sup>3+</sup>,Er<sup>3+</sup>,Eu<sup>3+</sup> NPs (a), MWCNTs (b), MWCNTs-NaGdF<sub>4</sub>:Yb<sup>3+</sup>,Er<sup>3+</sup>,Eu<sup>3+</sup> NCs (c), and the standard cards for NaGdF<sub>4</sub>:Yb<sup>3+</sup>,Er<sup>3+</sup>,Eu<sup>3+</sup> NPs and MWCNTs as a reference.



**Fig. 2** SEM images of  $\text{NaGdF}_4\text{:Yb}^{3+},\text{Er}^{3+},\text{Eu}^{3+}$  NPs (a), MWCNTs (c), MWCNTs- $\text{NaGdF}_4\text{:Yb}^{3+},\text{Er}^{3+},\text{Eu}^{3+}$  NCs (d and e), the histogram of the nanoparticle size of  $\text{NaGdF}_4\text{:Yb}^{3+},\text{Er}^{3+},\text{Eu}^{3+}$  NPs (b) and EDS spectra of MWCNTs- $\text{NaGdF}_4\text{:Yb}^{3+},\text{Er}^{3+},\text{Eu}^{3+}$  NCs (f).

conversion efficiency.<sup>17</sup> To further investigate the elemental composition, the EDS spectrum of NCs is displayed in Fig. 2f, it is noted that the sample contains C, F, Na, Yb, Er, Gd and Au elements. There are two strong peaks of Au coming from the spraying gold process. Combined with the above SEM images, it is further proved that the MWCNTs- $\text{NaGdF}_4\text{:Yb}^{3+},\text{Er}^{3+},\text{Eu}^{3+}$  multifunctional NCs are successfully synthesized.

### 3.2 Up-conversion photoluminescence

Fig. 3a illustrates the UV-Vis absorption spectrum of MWCNTs in DI water and the up-conversion luminescence spectrum of  $\text{NaGdF}_4\text{:Yb}^{3+},\text{Er}^{3+},\text{Eu}^{3+}$  NPs under 980 nm laser irradiation at room temperature. The MWCNTs have intense wide absorption from 450 to 750 nm. In the up-conversion luminescence spectrum of NPs, there are six main emission peaks at 500–700 nm. The peaks at 523, 540 and 655 nm correspond to the  $^2\text{H}_{11/2} \rightarrow ^4\text{I}_{15/2}$ ,  $^4\text{S}_{3/2} \rightarrow ^4\text{I}_{15/2}$  and  $^4\text{F}_{9/2} \rightarrow ^4\text{I}_{15/2}$  transitions of  $\text{Er}^{3+}$  ions, and the peaks at 589, 615 and 695 nm correspond to the  $^5\text{D}_0 \rightarrow ^7\text{F}_1$ ,  $^5\text{D}_0 \rightarrow ^7\text{F}_2$  and  $^5\text{D}_0 \rightarrow ^7\text{F}_4$  transitions of  $\text{Eu}^{3+}$  ions. As shown in Fig. 3b, we compared the up-conversion emission spectra of NPs and NCs at room temperature under 980 nm laser irradiation. The position of the up-conversion peaks in NCs is in accordance with that of the pure NPs, implying that the up-conversion processes have not

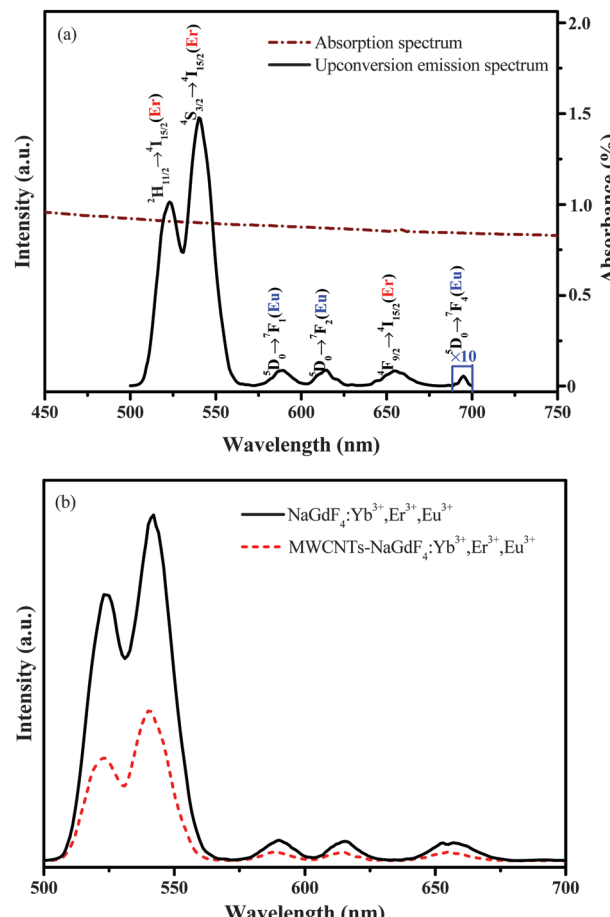


**Fig. 3** UV-Vis spectra of MWCNTs and up-conversion spectra of  $\text{NaGdF}_4\text{:Yb}^{3+},\text{Er}^{3+},\text{Eu}^{3+}$  NPs in water (a), up-conversion emission spectra of  $\text{NaGdF}_4\text{:Yb}^{3+},\text{Er}^{3+},\text{Eu}^{3+}$  NPs and MWCNTs- $\text{NaGdF}_4\text{:Yb}^{3+},\text{Er}^{3+},\text{Eu}^{3+}$  NCs under irradiation with a 980 nm laser (b).

changed by introduction of MWCNTs. It can be seen that the intensity of the up-conversion emission spectrum in NPs is obviously decreased when the MWCNTs are introduced into the nanocomposites. There are two main reasons accounting for this phenomenon, on the one hand, the MWCNTs can absorb the 980 nm laser excitation light and the up-conversion emissions of NPs. On the other hand, the volume of the sample pool is fixed when the MWCNTs are introduced into the nanocomposites, and the content of NPs decreases. At last, one can see that the MWCNTs- $\text{NaGdF}_4\text{:Yb}^{3+},\text{Er}^{3+},\text{Eu}^{3+}$  NCs exhibit mainly green emission under excitation with a 980 nm laser.

### 3.3 Down-conversion photoluminescence and lifetime

In order to investigate the down-conversion luminescence, the photoluminescence properties of  $\text{NaGdF}_4\text{:Yb}^{3+},\text{Er}^{3+},\text{Eu}^{3+}$  NPs and MWCNTs- $\text{NaGdF}_4\text{:Yb}^{3+},\text{Er}^{3+},\text{Eu}^{3+}$  NCs were examined. In the excitation spectrum of  $\text{NaGdF}_4\text{:Yb}^{3+},\text{Er}^{3+},\text{Eu}^{3+}$  NPs (Fig. 4 left) monitored at the wavelength of 615 nm, there are three main excitation peaks. The sharp excitation peak at 274 nm is assigned to the f-f transition of  $\text{Gd}^{3+}$ , the peaks from 300 to 450 nm are due to the f-f transition of  $\text{Eu}^{3+}$ , which is centered at 318 nm

( $^7F_0 \rightarrow ^5H_3$ ) and 394 nm ( $^7F_0 \rightarrow ^5L_6$ ). The presence of  $Gd^{3+}$  transition (274 nm) indicates that the efficient energy transfer appears between  $Gd^{3+}$  and  $Eu^{3+}$ . For the emission spectra (right), upon excitation with 274 nm, the emission spectra of NPs and NCs exhibit two characteristic peaks of  $Eu^{3+}$ , whose positions are at 589 and 615 nm. As shown to us, the MWCNTs have intense wide absorption from 450 nm to 700 nm (Fig. 3a). When introducing the MWCNTs to the nanocomposites, the intensity of the down-conversion emission is reduced than that of pure NPs. It can be explained by the fact that the down-conversion emission peaks of  $Eu^{3+}$  ions are completely overlapped with the absorption spectrum of MWCNTs; it can absorb light which is emitted from the NPs. The position of the down-conversion spectral peaks in NCs match with that of the pure NPs, moreover, several emission bands centered at 465, 489, 511, 536, 556, 584, 589, 615 and 695 nm can be assigned to the  $^5D_2 \rightarrow ^7F_0$ ,  $^5D_2 \rightarrow ^7F_2$ ,  $^5D_2 \rightarrow ^7F_3$ ,  $^5D_1 \rightarrow ^7F_1$ ,  $^5D_1 \rightarrow ^7F_2$ ,  $^5D_1 \rightarrow ^7F_3$ ,  $^5D_0 \rightarrow ^7F_1$ ,  $^5D_0 \rightarrow ^7F_2$  and  $^5D_0 \rightarrow ^7F_4$  transitions of  $Eu^{3+}$ , respectively. The MWCNTs–NaGdF<sub>4</sub>:Yb<sup>3+</sup>,Er<sup>3+</sup>,Eu<sup>3+</sup> NCs exhibit red emission under irradiation with 274 nm UV light.

The luminescence decay time curves for the  $^5D_0 \rightarrow ^7F_2$  (615 nm) transition of  $Eu^{3+}$  ions in NaGdF<sub>4</sub>:Yb<sup>3+</sup>,Er<sup>3+</sup>,Eu<sup>3+</sup> NPs and MWCNTs–NaGdF<sub>4</sub>:Yb<sup>3+</sup>,Er<sup>3+</sup>,Eu<sup>3+</sup> NCs were examined at room temperature. Fig. 5 displays the log normalized decay of  $^5D_0 \rightarrow ^7F_2$  at 615 nm. One can see that the decay curves of  $Eu^{3+}$  can be best fitted to the single exponential function of  $I = I_0 + A \exp(-t/\tau)$ . Here,  $I$  and  $I_0$  correspond to the luminescence intensities at time  $t$  and 0, while  $\tau$  corresponds to the luminescence decay time. From Fig. 5, it is obvious that the decay time for the  $^5D_0 \rightarrow ^7F_2$  transition of  $Eu^{3+}$  ions decreases from 5.53 ms to 5.18 ms in the absence and presence of MWCNTs, respectively. The results show that the presence of MWCNTs can hardly reduce the emission lifetime of  $Eu^{3+}$  ions in MWCNTs–NaGdF<sub>4</sub>:Yb<sup>3+</sup>,Er<sup>3+</sup>,Eu<sup>3+</sup> NCs.

#### 3.4 CIE chromaticity coordinates

The Commission Internationale de L'Eclairage (CIE) chromaticity coordinates of NaGdF<sub>4</sub>:Yb<sup>3+</sup>,Er<sup>3+</sup>,Eu<sup>3+</sup> NPs and

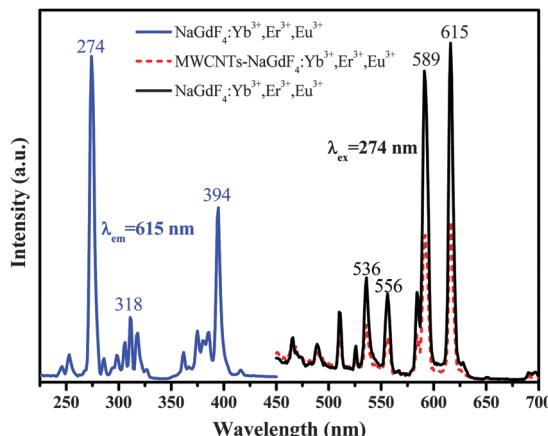


Fig. 4 Excitation (left) and emission (right) spectra of NaGdF<sub>4</sub>:Yb<sup>3+</sup>,Er<sup>3+</sup>,Eu<sup>3+</sup> NPs and MWCNTs–NaGdF<sub>4</sub>:Yb<sup>3+</sup>,Er<sup>3+</sup>,Eu<sup>3+</sup> NCs.

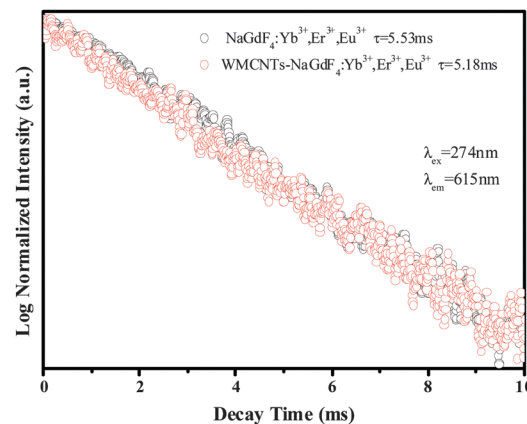


Fig. 5 Decay curves of  $Eu^{3+}$  ions in NaGdF<sub>4</sub>:Yb<sup>3+</sup>,Er<sup>3+</sup>,Eu<sup>3+</sup> NPs and MWCNTs–NaGdF<sub>4</sub>:Yb<sup>3+</sup>,Er<sup>3+</sup>,Eu<sup>3+</sup> NCs.

MWCNTs–NaGdF<sub>4</sub>:Yb<sup>3+</sup>,Er<sup>3+</sup>,Eu<sup>3+</sup> NCs are presented under different excitation wavelengths, as marked in the CIE chromaticity diagram of Fig. 6, which were calculated according to the relevant emission spectra. The CIE chromaticity coordinates of NPs and NCs excited by 980 nm are determined to be (0.225, 0.674) and (0.221, 0.740), located in the green region (points b and a), and the green emission light can be observed by the naked eye. Similarly, the CIE coordinates of (0.440, 0.368) and (0.493, 0.374) were obtained under 274 nm UV-lamp excitation (points c and d). This result further demonstrates that the MWCNTs–NaGdF<sub>4</sub>:Yb<sup>3+</sup>,Er<sup>3+</sup>,Eu<sup>3+</sup> NCs can exhibit bright green or red emission under irradiation with 980 nm laser or 274 nm UV-lamp light.

#### 3.5 Energy transfer processes

The schematic diagram for the possible mechanism of the energy transfer (ET) process in Yb<sup>3+</sup>,Er<sup>3+</sup>,Eu<sup>3+</sup> tri-doped NaGdF<sub>4</sub> is shown in Fig. 7. The Yb<sup>3+</sup> ions were successfully excited under irradiation with a 980 nm laser from the ground state of

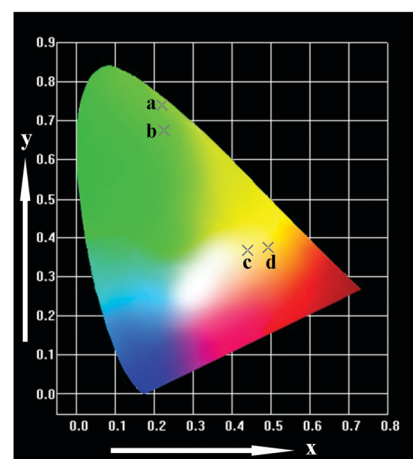


Fig. 6 CIE chromaticity diagram for NaGdF<sub>4</sub>:Yb<sup>3+</sup>,Er<sup>3+</sup>,Eu<sup>3+</sup> NPs (b and c) and MWCNTs–NaGdF<sub>4</sub>:Yb<sup>3+</sup>,Er<sup>3+</sup>,Eu<sup>3+</sup> NCs (a and d) excited at 980 and 274 nm.

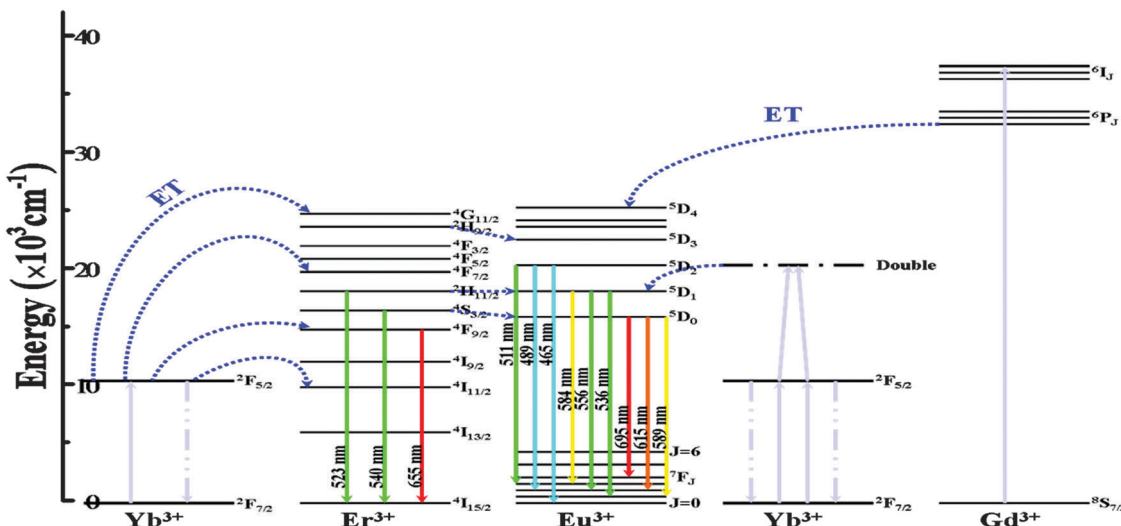


Fig. 7 Energy level diagram of  $\text{Yb}^{3+}$ ,  $\text{Er}^{3+}$ ,  $\text{Eu}^{3+}$  and  $\text{Gd}^{3+}$  ions with possible schemes of energetic processes.

$^2\text{F}_{7/2}$  to the excited state of  $^2\text{F}_{5/2}$ . And there are four effective ET processes from  $\text{Yb}^{3+}$  ions in the  $^2\text{F}_{5/2}$  excited state to  $\text{Er}^{3+}$  ions which are populated  $^4\text{I}_{11/2}$ ,  $^4\text{F}_{9/2}$ ,  $^4\text{F}_{7/2}$  and  $^4\text{G}_{11/2}$  excited energy levels, respectively, with the redundant energy dissipated by phonons. As we all have known,  $\text{Eu}^{3+}$  cannot absorb the 980 nm laser excitation directly, but it can absorb the energy transferred from the excited state of  $\text{Yb}^{3+}$  ions and  $\text{Er}^{3+}$  ions. And the ET between  $\text{Yb}^{3+}$  and  $\text{Eu}^{3+}$  ions occurs through the double excited energy level of  $\text{Yb}^{3+}$  ions ( $^2\text{F}_{5/2}$ ) by cooperative sensitization and results in  $^5\text{D}_0 \rightarrow ^7\text{F}_J$  emissions at about 600 nm.<sup>35,36</sup> It is noticed that the energy levels of  $^2\text{H}_{9/2}$ ,  $^2\text{H}_{11/2}$  and  $^4\text{S}_{3/2}$  of  $\text{Er}^{3+}$  are little higher than those of  $^5\text{D}_3$ ,  $^5\text{D}_1$  and  $^5\text{D}_0$  of  $\text{Eu}^{3+}$  ions which enables ET through the nonradiative processes. Finally, the excited states of  $\text{Er}^{3+}$  ions from the  $^2\text{H}_{11/2}$  and  $^4\text{S}_{3/2}$  levels relax radioactively to the ground state which leads to green emission at 523 and 540 nm, similarly, the  $^4\text{F}_{9/2} \rightarrow ^4\text{I}_{15/2}$  red emission at 655 nm of  $\text{Er}^{3+}$ , and  $\text{Eu}^{3+}$  of the  $^5\text{D}_0 \rightarrow ^7\text{F}_1$ ,  $^5\text{D}_0 \rightarrow ^7\text{F}_2$  and  $^5\text{D}_0 \rightarrow ^7\text{F}_4$  transitions of  $\text{Eu}^{3+}$ , that is yellow emission at 589 nm, orange emission at 615 nm and red emission at 695 nm.<sup>45</sup> But we can see that in the up-conversion emission spectra of  $\text{NaGdF}_4\text{-Yb}^{3+},\text{Er}^{3+},\text{Eu}^{3+}$  NPs and MWCNTs– $\text{NaGdF}_4\text{-Yb}^{3+},\text{Er}^{3+},\text{Eu}^{3+}$  NCs, the peaks are strong in the green emission bands. They only emit green emission, as indicated in Fig. 3b. And then, we discuss the down-conversion emission, the ET between the  $\text{Gd}^{3+}$  and  $\text{Eu}^{3+}$  ions can occur under excitation with 274 nm UV light.<sup>41,42</sup> The emission bands of  $\text{Eu}^{3+}$  centered at 589 and 584 nm are assigned to the  $^5\text{D}_0 \rightarrow ^7\text{F}_1$  and  $^5\text{D}_1 \rightarrow ^7\text{F}_3$  transitions for yellow light, the peak at 615 nm assigned to the  $^5\text{D}_0 \rightarrow ^7\text{F}_2$  transition for orange light, the peak at 695 nm assigned to the  $^5\text{D}_0 \rightarrow ^7\text{F}_4$  transition for red light, the peaks at 536, 556 and 511 nm assigned to the  $^5\text{D}_1 \rightarrow ^7\text{F}_1$ ,  $^5\text{D}_1 \rightarrow ^7\text{F}_2$  and  $^5\text{D}_2 \rightarrow ^7\text{F}_3$  transitions for green light, the peaks at 465 and 489 nm assigned to the  $^5\text{D}_2 \rightarrow ^7\text{F}_0$  and  $^5\text{D}_2 \rightarrow ^7\text{F}_2$  transitions for cyan light, respectively. We can observe that the  $\text{Eu}^{3+}$  ions emit red light under excitation with 274 nm UV light, this is because of the fact that the peaks are strongly centered at 589 and 615 nm as observed from Fig. 4. Whether it is

up-conversion or down-conversion luminescence, when the MWCNTs and  $\text{NaGdF}_4\text{-Yb}^{3+},\text{Er}^{3+},\text{Eu}^{3+}$  NPs were compounded together, the luminescence became weak because MWCNTs have intense wide absorption from 450 nm to 750 nm, and they can absorb the excitation light of source and the emission light of NPs.

### 3.6 Photothermal properties

As mentioned earlier, the MWCNTs are effective photothermal conversion agents, they can be used as molecular antennae to absorb the NIR light region and convert the NIR light to heat through the photothermal effect, so they have been widely used in PTT. To further prove the photothermal effect of the MWCNTs– $\text{NaGdF}_4\text{-Yb}^{3+},\text{Er}^{3+},\text{Eu}^{3+}$  NCs, we exposed the solution of samples to a 980 nm NIR laser irradiation at a power density of  $1.2 \text{ W cm}^{-2}$  for 10 min, and examined the temperature changes. As shown in Fig. 8a, we observe that the temperature of the solution is significantly increased; the temperature of DI water and NP solution only increases to  $34.3^\circ\text{C}$  and  $36.5^\circ\text{C}$  under irradiation for 10 min, but the temperature of NC aqueous solution with  $0.3 \text{ mg mL}^{-1}$  is increased from  $20.0^\circ\text{C}$  to  $47.1^\circ\text{C}$ . However, in marked contrast to the small temperature changes of DI water and the NP sample, the temperature of the aqueous solution increases slightly from NPs and mainly from MWCNTs. From Fig. 8b, it can be seen that with increasing concentration of NCs, the final temperature of the aqueous solution increases. It indicates that the MWCNTs– $\text{NaGdF}_4\text{-Yb}^{3+},\text{Er}^{3+},\text{Eu}^{3+}$  NCs have an outstanding photothermal conversion property and the temperature can be controlled by adjusting the concentration of NCs. In view of the fact that the photothermal conversion property efficiency of MWCNTs– $\text{NaGdF}_4\text{-Yb}^{3+},\text{Er}^{3+},\text{Eu}^{3+}$  NCs is significant, they can be used as a prominent photothermal agent.

### 3.7 Magnetic properties

To compare the magnetic behavior of MWCNTs– $\text{NaGdF}_4\text{-Yb}^{3+},\text{Er}^{3+},\text{Eu}^{3+}$  NCs, the pure  $\text{NaGdF}_4\text{-Yb}^{3+},\text{Er}^{3+},\text{Eu}^{3+}$  NPs have been

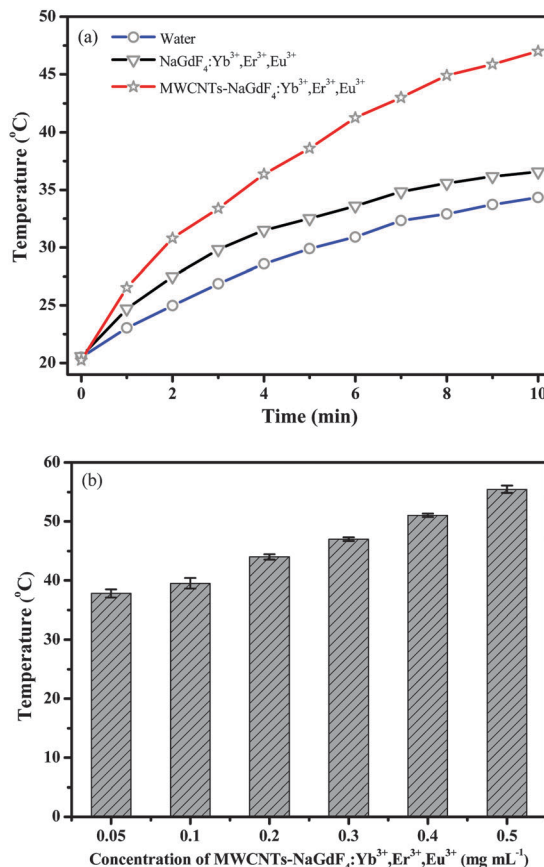


Fig. 8 Temperature of water, NaGdF<sub>4</sub>:Yb<sup>3+</sup>,Er<sup>3+</sup>,Eu<sup>3+</sup> NPs and MWCNTs–NaGdF<sub>4</sub>:Yb<sup>3+</sup>,Er<sup>3+</sup>,Eu<sup>3+</sup> NCs as a function of excitation time (a), the final temperature of different concentrations of MWCNTs–NaGdF<sub>4</sub>:Yb<sup>3+</sup>,Er<sup>3+</sup>,Eu<sup>3+</sup> NCs after excitation for 10 min with 980 nm laser (b).

prepared under the same reaction conditions. They were examined in the fields between  $-20$  and  $20$  kOe using a VSM at room temperature, the magnetization curves are shown in Fig. 9. The as-synthesized NCs and NPs both show paramagnetic properties due to no coercivity or remanence; the magnetic hysteresis loops of NCs and NPs show that the magnetization is found to be about  $1.5509$  and  $1.9323$  emu g<sup>-1</sup> at  $20$  kOe, respectively, which approach the value reported for nanocomposites used for ordinary bioseparation.<sup>46,47</sup> Comparing the magnetization values of both NPs and NCs, it can be found that the magnetization value reduces to about  $0.38$  emu g<sup>-1</sup>, because the presence of MWCNTs leads to a low content of NPs in the NCs. Therefore, the magnetization of the MWCNTs–NaGdF<sub>4</sub>:Yb<sup>3+</sup>,Er<sup>3+</sup>,Eu<sup>3+</sup> NCs is slightly decreased in comparison.

### 3.8 Cell viability assay

To examine the utility of the probe in biological systems, it was applied to Hep-2 cells. It is especially important to evaluate the cytotoxicity of the MWCNTs–NaGdF<sub>4</sub>:Yb<sup>3+</sup>,Er<sup>3+</sup>,Eu<sup>3+</sup> NCs by 3-(4,5-dimethylthiazol-2-yl)-2,5-diphenyltetrazolium bromide (MTT) assay on Hep-2 cells. As displayed in Fig. 10, Hep-2 cells were incubated with a series of concentration of NCs for 12 and 24 h. We can see that there are no evident changes in Hep-2 cell

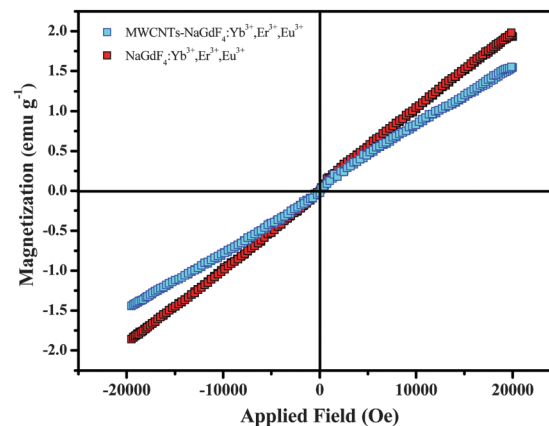


Fig. 9 Room-temperature magnetization curves of MWCNTs–NaGdF<sub>4</sub>:Yb<sup>3+</sup>,Er<sup>3+</sup>,Eu<sup>3+</sup> NCs and pure NaGdF<sub>4</sub>:Yb<sup>3+</sup>,Er<sup>3+</sup>,Eu<sup>3+</sup> NPs.

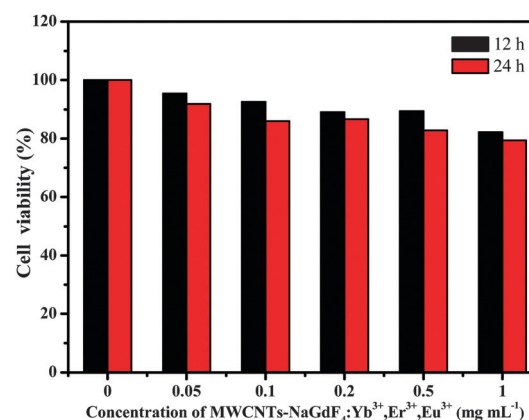
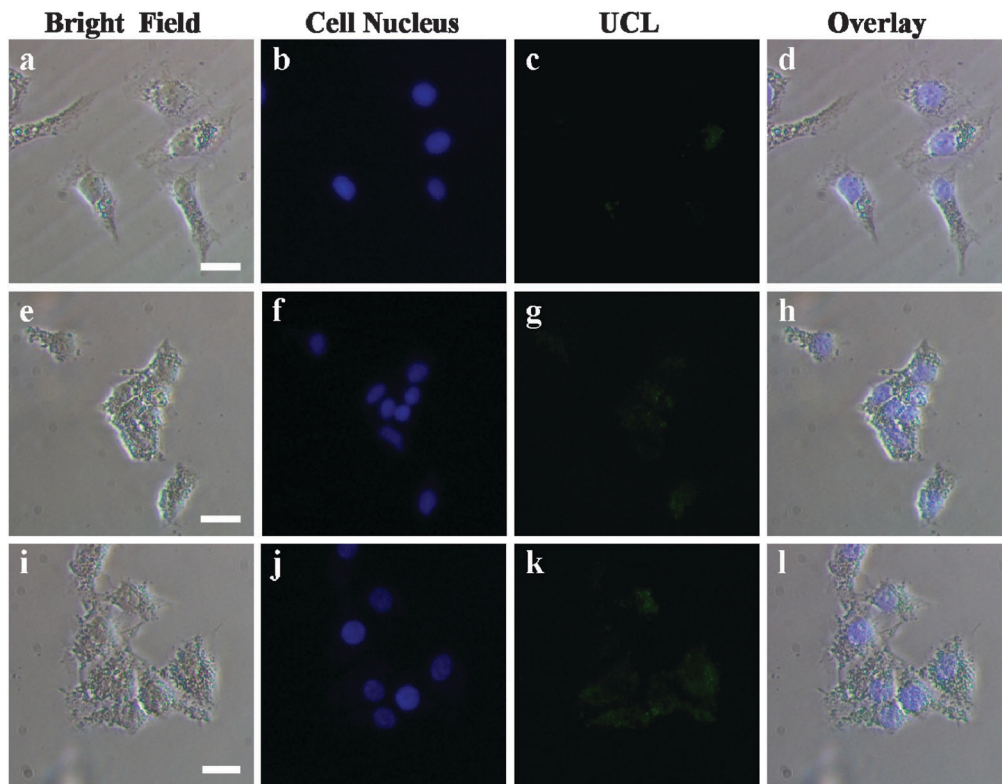


Fig. 10 Viability of Hep-2 cells after incubating with different concentrations of MWCNTs–NaGdF<sub>4</sub>:Yb<sup>3+</sup>,Er<sup>3+</sup>,Eu<sup>3+</sup> NCs for 12 and 24 h, and quantitative assays using the standard MTT assay.

viability when incubated with the NCs for 12 and 24 h. It should be noted that the NCs displayed negligible cytotoxicity even after incubation at high doses of NCs ( $1$  mg mL<sup>-1</sup>). The MTT assay results indicate that the MWCNTs–NaGdF<sub>4</sub>:Yb<sup>3+</sup>,Er<sup>3+</sup>,Eu<sup>3+</sup> NCs show excellent biocompatibility and potential biological application.

### 3.9 Fluorescence imaging

The MWCNTs–NaGdF<sub>4</sub>:Yb<sup>3+</sup>,Er<sup>3+</sup>,Eu<sup>3+</sup> NCs were allowed to uptake by the Hep-2 cells. And the images were investigated by inverted up-conversion luminescence microscopy (UCLM). The Hep-2 cells were incubated with NCs ( $0.3$  mg mL<sup>-1</sup>) for different time periods (10 min, 1 h and 6 h) at  $37$  °C and the up-conversion luminescence images were examined with infrared laser excitation at  $980$  nm. Fig. 11 illustrates the bright field, cell nucleus (being dyed in blue by DAPI for visualization), up-conversion luminescence (UCL) images and merged images of Hep-2 cells. We used time course UCLM to examine the interaction between the Hep-2 cells and the NCs. As shown in Fig. 11a–d, one can see that in the first 10 min, only a few NCs (shown in green) could be internalized by Hep-2 cells. After incubation for 1 h (Fig. 11e–h), the green-emission gradually



**Fig. 11** Inverted luminescence microscopy images of Hep-2 cells incubated with MWCNTs–NaGdF<sub>4</sub>:Yb<sup>3+</sup>,Er<sup>3+</sup>,Eu<sup>3+</sup> NCs for 10 min (a–d), 1 h (e–h) and 6 h (i–l) at 37 °C. Each series can be classified into bright field images, cell nucleus, up-conversion luminescence images (UCL) and the overlay of the above three, respectively. All scale bars are of 100 μm.

increased in the cytoplasm. As the time is prolonged to 6 h (Fig. 11i–l), a stronger UCL signal could be seen, indicating that a large number of NCs were distributed in the cytoplasmic region of the Hep-2 cells. This indicates that the as-prepared MWCNTs–NaGdF<sub>4</sub>:Yb<sup>3+</sup>,Er<sup>3+</sup>,Eu<sup>3+</sup> NCs were well accumulated and taken up in the cell cytoplasm, and then they can be used as an excellent fluorescence imaging probe for cell imaging<sup>48–50</sup> and monitoring the endocytosis process of cells.<sup>51</sup>

## 4 Conclusions

In summary, we have prepared novel magnetic/thermal/optical multifunctional MWCNTs–NaGdF<sub>4</sub>:Yb<sup>3+</sup>,Er<sup>3+</sup>,Eu<sup>3+</sup> NCs through a facile method. The NaGdF<sub>4</sub>:Yb<sup>3+</sup>,Er<sup>3+</sup>,Eu<sup>3+</sup> NPs were coated on the surface of MWCNTs. The position of the emission peaks in NCs is in accordance with pure NaGdF<sub>4</sub>:Yb<sup>3+</sup>,Er<sup>3+</sup>,Eu<sup>3+</sup> NPs, which indicates that their emission processes have not changed upon connecting with MWCNTs. In addition, this kind of Yb<sup>3+</sup>,Er<sup>3+</sup>,Eu<sup>3+</sup> ions tri-doped NaGdF<sub>4</sub> NP system displays novel dual-mode luminescence, including up- and down-conversion emissions under different excitation wavelengths, as well as excellent magnetic properties. The solution temperature of MWCNTs–NaGdF<sub>4</sub>:Yb<sup>3+</sup>,Er<sup>3+</sup>,Eu<sup>3+</sup> NCs is obviously increased under excitation with 980 nm laser for 10 min, owing to the photothermal conversion property. Simultaneously, we observe that the temperature can be changed by

varying the concentration of NCs. The MTT assay illustrates that the NCs show low cytotoxicity and meritorious biocompatibility. Meanwhile, the as-prepared NCs can be used as excellent up- and down-conversion luminescent probes for cell imaging. Overall, the multifunctional MWCNTs–NaGdF<sub>4</sub>:Yb<sup>3+</sup>,Er<sup>3+</sup>,Eu<sup>3+</sup> NCs could be used for highly promising multi-aspect applications such as MRI, fluorescence imaging, PTT, targeted drug delivery and magnetic separation in biomedical and environmental science fields.

## Acknowledgements

This work was supported by the National Natural Science Foundation of P. R. China (NSFC) (Grant No. 51072026 and 50972020) and the development of science and technology plan projects of Jilin province (Grant No. 20130206002 GX).

## Notes and references

- S. Iijima, *Nature*, 1991, **354**, 56–58.
- S. Morales-Torres, T. L. S. Silva, L. M. Pastrana-Martinez, A. T. S. C. Branda, J. L. Figueiredo and A. M. T. Silva, *Phys. Chem. Chem. Phys.*, 2014, **16**, 12237–12250.
- S. Niyogi, M. A. Hamon, H. Hu, B. Zhao, P. Bhowmik, R. Sen, M. E. Itkis and R. C. Haddon, *Acc. Chem. Res.*, 2002, **35**, 1105–1113.

- 4 Q. Cheng, J. Tang, J. Ma, H. Zhang, N. Shinya and L.-C. Qin, *Phys. Chem. Chem. Phys.*, 2011, **13**, 17615–17624.
- 5 H. Ma, L. Pan, Q. Zhao and W. Peng, *Nanoscale*, 2013, **5**, 1153–1158.
- 6 C. J. Gannon, P. Cherukuri, B. I. Yakobson, L. Cognet, J. S. Kanzius, C. Kittrell, R. B. Weisman, M. Pasquali, H. K. Schmidt, R. E. Smalley and S. A. Curley, *Cancer*, 2007, **110**, 2654–2665.
- 7 R. Moradi, S. A. Sebt, H. Karimi-Maleh, R. Sadeghi, F. Karimi, A. Bahari and H. Arabi, *Phys. Chem. Chem. Phys.*, 2013, **15**, 5888–5897.
- 8 H.-C. Wu, X. Chang, L. Liu, F. Zhao and Y. Zhao, *J. Mater. Chem.*, 2010, **20**, 1036–1052.
- 9 A. Bianco, K. Kostarelos and M. Prato, *Chem. Commun.*, 2011, **47**, 10182–10188.
- 10 R. K. Singh, K. D. Patel, J. J. Kim, T. H. Kim, J. H. Kim, U. S. Shin, E. J. Lee, J. C. Knowles and H. W. Kim, *ACS Appl. Mater. Interfaces*, 2014, **6**, 2201–2208.
- 11 K. T. Al-Jamal, H. Nerl, K. H. Muller, H. Ali-Boucetta, S. Li, P. D. Haynes, J. R. Jinschek, M. Prato, A. Bianco, K. Kostarelos and A. E. Porter, *Nanoscale*, 2011, **3**, 2627–2635.
- 12 J. Bartelmess, S. J. Quinn and S. Giordani, *Chem. Soc. Rev.*, 2015, **44**, 4672–4698.
- 13 Y. Huang, M. Shi, K. Hu, S. Zhao, X. Lu, Z.-F. Chen, J. Chen and H. Liang, *J. Mater. Chem. B*, 2013, **1**, 3470–3476.
- 14 X. Huang, I. H. El-Sayed, W. Qian and M. A. El-Sayed, *J. Am. Chem. Soc.*, 2006, **128**, 2115–2120.
- 15 A. M. Gobin, M. H. Lee, N. J. Halas, W. D. James, R. A. Drezek and J. L. West, *Nano Lett.*, 2007, **7**, 1929–1934.
- 16 D. Boyer, P. Tamarat, A. Maali, B. Lounis and M. Orrit, *Science*, 2002, **297**, 1160–1163.
- 17 Y. Hu, L. Meng, L. Niu and Q. Lu, *ACS Appl. Mater. Interfaces*, 2013, **5**, 4586–4591.
- 18 Y. Song, G. Liu, X. Dong, J. Wang, W. Yu and J. Li, *RSC Adv.*, 2014, **4**, 62802–62808.
- 19 B. Dong, S. Xu, J. Sun, S. Bi, D. Li, X. Bai, Y. Wang, L. Wang and H. Song, *J. Mater. Chem.*, 2011, **21**, 6193–6200.
- 20 S. Iijima and T. Ichihashi, *Nature*, 1993, **363**, 603–605.
- 21 P. Singh, C. Samorì, F. M. Toma, C. Bussy, A. Nunes, K. T. Al-Jamal, C. Ménard-Moyon, M. Prato, K. Kostarelos and A. Bianco, *J. Mater. Chem.*, 2011, **21**, 4850–4860.
- 22 H. Hekmatara, M. Seifi, K. Forooraghi and S. Mirzaee, *Phys. Chem. Chem. Phys.*, 2014, **16**, 24069–24075.
- 23 Z. Cheng, R. Chai, P. Ma, Y. Dai, X. Kang, H. Lian, Z. Hou, C. Li and J. Lin, *Langmuir*, 2013, **29**, 9573–9580.
- 24 N. W. Kam, M. O'Connell, J. A. Wisdom and H. Dai, *Proc. Natl. Acad. Sci. U. S. A.*, 2005, **102**, 11600–11605.
- 25 C. Fabbro, H. Ali-Boucetta, T. Da Ros, K. Kostarelos, A. Bianco and M. Prato, *Chem. Commun.*, 2012, **48**, 3911–3926.
- 26 G. Chen, T. Y. Ohulchansky, W. C. Law, H. Agren and P. N. Prasad, *Nanoscale*, 2011, **3**, 2003–2008.
- 27 J. Zhou, Y. Sun, X. Du, L. Xiong, H. Hu and F. Li, *Biomaterials*, 2010, **31**, 3287–3295.
- 28 Z.-L. Wang, J. H. Hao and H. L. W. Chan, *J. Mater. Chem.*, 2010, **20**, 3178–3185.
- 29 Q. Ju, D. Tu, Y. Liu, R. Li, H. Zhu, J. Chen, Z. Chen, M. Huang and X. Chen, *J. Am. Chem. Soc.*, 2012, **134**, 1323–1330.
- 30 G. Lamanna, A. Garofalo, G. Popa, C. Wilhelm, S. Begin-Colin, D. Felder-Flesch, A. Bianco, F. Gazeau and C. Menard-Moyon, *Nanoscale*, 2013, **5**, 4412–4421.
- 31 W. Xu, K. Kattel, J. Y. Park, Y. Chang, T. J. Kim and G. H. Lee, *Phys. Chem. Chem. Phys.*, 2012, **14**, 12687–12700.
- 32 S. Zeng, H. Wang, W. Lu, Z. Yi, L. Rao, H. Liu and J. Hao, *Biomaterials*, 2014, **35**, 2934–2941.
- 33 H. Guan, G. Liu, J. Wang, X. Dong and W. Yu, *Dalton Trans.*, 2014, **43**, 10801–10808.
- 34 T. Grzyb, A. Gruszczka, R. J. Wiglus, Z. Śniadecki, B. Idzikowski and S. Lis, *J. Mater. Chem.*, 2012, **22**, 22989–22997.
- 35 T. Grzyb, R. J. Wiglus, A. Gruszczka and S. Lis, *Dalton Trans.*, 2014, **43**, 17255–17264.
- 36 H. Lian, Y. Dai, D. Yang, Z. Cheng, C. Li, Z. Hou, M. Shang and J. Lin, *Nanoscale*, 2014, **6**, 9703–9712.
- 37 T. Grzyb, *RSC Adv.*, 2014, **4**, 2590–2595.
- 38 X. Wang, C.-S. Liu, T. Yu and X. Yan, *Phys. Chem. Chem. Phys.*, 2014, **16**, 13440–13446.
- 39 W. Wang, H. Song, X. Bai, Q. Liu and Y. Zhu, *Phys. Chem. Chem. Phys.*, 2011, **13**, 18023–18030.
- 40 T. Jung, H. L. Jo, S. H. Nam, B. Yoo, Y. Cho, J. Kim, H. M. Kim, T. Hyeon, Y. D. Suh, H. Lee and K. T. Lee, *Phys. Chem. Chem. Phys.*, 2015, **17**, 13201–13205.
- 41 S. Wang, J. Feng, S. Song and H. Zhang, *RSC Adv.*, 2014, **4**, 55897–55899.
- 42 G. Xiang, J. Zhang, Z. Hao, X. Zhang, G.-H. Pan, Y. Luo and H. Zhao, *CrystEngComm*, 2015, **17**, 3103–3109.
- 43 V. Kumar Rai, A. Pandey and R. Dey, *J. Appl. Phys.*, 2013, **113**, 083104.
- 44 L. Wang, X. Xue, H. Chen, D. Zhao and W. Qin, *Chem. Phys. Lett.*, 2010, **485**, 183–186.
- 45 J. Zhang, Z. Hao, J. Li, X. Zhang, Y. Luo and G. Pan, *Light: Sci. Appl.*, 2015, **4**, e239.
- 46 S. Y. Kim, K. Woo, K. Lim, K. Lee and H. S. Jang, *Nanoscale*, 2013, **5**, 9255–9263.
- 47 H. Guan, G. Liu, J. Wang, X. Dong and W. Yu, *New J. Chem.*, 2014, **38**, 4901–4907.
- 48 S. Wang, J. Feng, S. Song and H. Zhang, *CrystEngComm*, 2013, **15**, 7142–7151.
- 49 F. Wang, D. Banerjee, Y. Liu, X. Chen and X. Liu, *Analyst*, 2010, **135**, 1839–1854.
- 50 P. Yuan, Y. H. Lee, M. K. GnanaSammandhan, Z. Guan, Y. Zhang and Q.-H. Xu, *Nanoscale*, 2012, **4**, 5132–5137.
- 51 X. Liu, R. Deng, Y. Zhang, Y. Wang, H. Chang, L. Huang and X. Liu, *Chem. Soc. Rev.*, 2015, **44**, 1479–1508.